

Oscillatory properties of strange quark stars described by the vector MIT bag model

Luiz L. Lopes,^{1,*} José C. Jiménez,^{2,3} Luis B. Castro,^{4,*} and César V. Flores^{5,4,†}

¹*Centro Federal de Educação Tecnológica de Minas Gerais Campus VIII,
CEP 37.022-560, Varginha, MG, Brazil*

²*Departament of Astrophysics, Brazilian Center for Research in Physics (CBPF),
Rua Dr. Xavier Sigaud, 150, URCA, Rio de Janeiro CEP 22210-180, RJ, Brazil*

³*Universidad Tecnológica del Perú, Arequipa - Perú*

⁴*Universidade Federal do Maranhão, UFMA, Departamento de Física-CCET,
Campus Universitário do Bacanga, São Luís, CEP 65080-805 Maranhão, Brazil*

⁵*Universidade Estadual da Região Tocantina do Maranhão, UEMASUL,
Centro de Ciências Exatas, Naturais e Tecnológicas, Imperatriz, CEP 65901-480 Maranhão, Brazil*

We investigated the radial and non-radial fundamental (f) mode oscillations of self-bound (quark) stars obtained after employing the Vector MIT (vMIT) bag model. Within this model, we computed the equation of state for strange quark matter satisfying thermodynamic consistency. This allowed us to obtain the corresponding behavior of the speed of sound, mass-radius relation, and gravitational redshift. In particular, our choice of $G_V = 0.30 \text{ fm}^2$ produces masses and radii in agreement with recent astronomical data (e.g. from NICER and HESS J1731). In fact, we tested that variations of the remaining vMIT parameters slightly modify this conclusion. Then, we proceeded to compute the radial oscillation frequencies of the f -mode, which is tightly connected to the dynamical stability of these compact stars. We found that increments of the G_V parameter have a stabilizing property around the maximal-mass stars for a given stellar family. We also calculated the gravitational-wave frequencies of the non-radial f -mode. Our results show that they are restricted to be in the range (1.6 - 1.8) kHz for high-mass stars and to (1.5 - 1.6) kHz for low-mass stars. Finally, we propose a universal relation between these frequencies and the square root of the average density. All these last results are important in distinguishing strange stars from ordinary neutron stars in future gravitational-wave detections coming from compact sources with activated non-radial modes.

I. INTRODUCTION

Strange quark stars are self-bounded compact objects composed of deconfined quarks at their interiors. The theory of strange quark stars is based on the so-called Bodmer–Witten conjecture [1, 2], which assumes that ordinary matter, composed of protons and neutrons, may only be meta-stable phase, while the true ground state of strongly interacting matter would therefore consist of the so-called strange quark matter (SQM), i.e. matter constituted by deconfined up, down, and strange quarks.

Assuming that at least some of the observed pulsars can potentially be strange quark stars, in this work, we study some macroscopic and microscopic properties of these objects. Using the vMIT bag model [3, 4], we begin by studying the equation of state (EoS) and its corresponding speed of sound for different values of the (main) coupling G_V . Afterwards, using the EoS as input, we study their macroscopic observables such as the mass-radius relation and the gravitational redshift. We then probe if these SQM stars fulfill current observational constraints, e.g. for their maximal masses [5].

In addition to the macroscopic relations that can be studied via electromagnetic signals, e.g. X-ray data for the radii of these objects, additional information can be obtained from gravitational wave asteroseismology. A

gravitational wave (GW) signal is a ripple in the fabric of space-time being produced by the accelerated motion of massive astrophysical objects, e.g. binary systems composed of two neutron stars. In fact, GWs were already detected in an indirect form near the year 1970 by observing the period of pulsar PSR B1913+16. Interestingly, in September 2015, a direct detection was performed by the LIGO-Virgo collaboration. Since then, hundreds of events have been observed including the merging of binary neutron stars [6]. In 2019, the LIGO-Virgo-KAGRA collaboration was established and their observation run O4 is currently ongoing, with another run (O5) planned to be completed by the end of this decade. Last but not least, the next decade will mark the advent of third-generation terrestrial gravitational-wave observatories (Einstein Telescope [7] and Cosmic Explorer [8]), as well as space detectors like LISA, opening the milliHertz frequency window [9]. The scientific knowledge expected from such intense research is outstanding, from fundamental physics to astrophysics and cosmology.

One of the phenomena that can produce GWs is the non-radial oscillations of compact stars. These oscillations can be categorized into different modes: f -modes, p -modes (pressure modes), and g -modes (gravity modes). In this study, we focus our study on the f -modes, whose frequency and damping time are directly influenced by the EoS of dense matter. Therefore, these modes directly describe how matter behaves at extremely high densities found in the inner regions of neutron stars. In this sense, it is well known that one can gain valuable insights of the

* lopes@cefetmg.br

† cesar.vasquez@uemasul.edu.br

microphysics and composition of neutron stars by analyzing gravitational waves generated by f -modes, since they are more easily excited compared to the overtones [10].

In this work, Sec. II outlines the use of the vMIT bag model to compute the EoS for SQM. Section III then addresses the calculation of equilibrium configurations for each SQM star, followed by the presentation of mass-radius relationship curves for all our stellar models of self-bound matter. In Sec. IV, we compute the fundamental radial oscillation mode to ensure our study is restricted to dynamically stable stars. In Sec. V, we give a universal relation connecting focus, the quadrupolar f -mode and the average density at the SQM star interiors. This is relevant since it is the most studied mode in the field of gravitational wave astronomy, thus being a promising source of gravitational radiation. Finally, Sec. VI presents our summary and conclusions.

II. THE VECTOR MIT BAG MODEL

The vector MIT bag model is an extension of the original MIT bag model [11] that incorporates some features of the quantum Hadrodynamics (QHD) [12]. In its original form, the MIT bag model considers that each baryon is composed of three non-interacting quarks inside a bag. The bag, in turn, corresponds to an infinite potential that confines the quarks. As a consequence, the quarks are free inside the bag and are forbidden to reach its exterior. All the information about the strong force relies on the bag pressure value, which mimics the vacuum pressure.

In the vector MIT bag model, the quarks are still confined inside the bag, but now they interact with each other through a vector meson exchange. This vector meson plays a role analog to the ω meson of the QHD [12]. Moreover, if one desires, the contribution of the Dirac sea can be taken into account through a self-interaction of the vector meson [13], although we do not follow this path in the present work, once its presence softens the EoS. Our Lagrangian of the vector MIT bag model, therefore, consists of the Lagrangian of the original MIT, plus the Yukawa-type Lagrangian of the vector field exchange. We must also add the mesonic mass term to maintain the thermodynamic consistency. It then reads [3, 4]:

$$\mathcal{L} = \mathcal{L}_{\text{MIT}} + \mathcal{L}_V, \quad (1)$$

where

$$\mathcal{L}_{\text{MIT}} = \sum_i \{\bar{\psi}_i [i\gamma^\mu \partial_\mu - m_i] \psi_i - B\} \Theta(\bar{\psi}_i \psi_i), \quad (2)$$

$$\mathcal{L}_V = \sum_i \{\bar{\psi}_i g_{iV} (\gamma^\mu V_\mu) \psi_i - \frac{1}{2} m_V^2 V^\mu V_\mu\} \Theta(\bar{\psi}_i \psi_i), \quad (3)$$

where ψ_i is the Dirac quark field, B is the constant vacuum pressure, m_V is the mass of the V_μ mesonic field, g_{iV}

is the coupling constant of the quark i with the meson V_μ . The $\Theta(\bar{\psi}_i \psi_i)$ is the Heaviside step function included to assure that the quarks exist only confined to the bag.

Applying the mean-field approximation (MFA) [12], and the Euler-Lagrange equations, we can obtain the energy eigenvalue for the quark fields, and the equation of motion for the mesonic $V_0 = \langle V_\mu \rangle \delta_0^\mu$ field:

$$E_i = \sqrt{m_i^2 + k_i^2} + g_{iV} V_0 \quad (4)$$

$$m_V^2 V_0 = \sum_i g_{iV} n_i, \quad (5)$$

$$n_i = \gamma_i \frac{k_f^3}{3\pi^2} \quad (6)$$

where n_i is the number density of the i -th quark and $\gamma_i = 6 = (3 \times 2)$ due to the number of colors and spin projections. Moreover, at $T = 0$, the energy eigenvalue is also the chemical potential (μ). To construct an EoS in the MFA, we now consider the Fermi-Dirac distribution of the quarks, and the Hamiltonian for the vector field and the bag pressure value, $\mathcal{H} = -\langle \mathcal{L} \rangle$. We obtain:

$$\varepsilon_i = \frac{\gamma_i}{2\pi^2} \int_0^{k_f} E_i k^2 dk, \quad (7)$$

$$\varepsilon = \sum_i \varepsilon_i + B - \frac{1}{2} m_V^2 V_0^2. \quad (8)$$

The last term of equation (8) being absent in Refs. [14–16] is crucial to kept the thermodynamic consistency of the model. To construct an electrically neutral, beta-stable matter, leptons are added as a free Fermi gas. The pressure is obtained via the thermodynamic relation, $p = \sum_i \mu_i n_i - \varepsilon$, where the sum runs over all the fermions.

In the following, we redefine $G_V \equiv (g_{uV}/m_V)^2$ and define $X_V \equiv (g_{sV}/g_{uV})$. Here, we use a universal coupling for X_V , $X_V = 1.0$, in opposition to $X_V = 0.4$ predicted by the symmetry group and used in Ref [17, 18]. A universal coupling produces more massive stars for the same value of G_V . The mass values utilized in this work are the same as suggested in Refs. [3, 4]; $m_u = m_d = 4 \text{ MeV}$ and $m_s = 95 \text{ MeV}$.

Now, the values of G_V and the bag are not fully independent. For the SM hypothesis to be true, the energy per baryon of the deconfined phase (for $p = 0$ and $T = 0$) must be lower than the nonstrange infinite baryonic matter. Or explicitly [1, 2]:

$$E_{(uds)}/A < 930 \text{ MeV}, \quad (9)$$

at the same time, the nonstrange matter still needs to have an energy per baryon higher than the one of non-strange infinite baryonic matter, otherwise, protons and neutrons would decay into u and d quarks:

$$E_{(ud)}/A > 930 \text{ MeV}. \quad (10)$$

Therefore, both, eq. (9) and (10) must simultaneous be true. For a given value of G_V , the values of the bag that satisfy the SQM hypothesis form the so-called stability window. The stability window for $G_V = 0.0$ up to 0.3 fm^2 is presented as Fig. 4 in Ref. [3]. The G_V and the bag act together in a positive feedback way: If we increase the G_V we increase the maximum mass of the star but also reduce the value of the bag inside the stability window. At the same time, lower values of the bag produce an additional increase in the maximum mass.

We use here three different values of G_V , 0.18, 0.24, and 0.30 fm^2 , and in order to satisfy the SQM hypothesis we see that the corresponding values for the Bag constant are: $B^{1/4} = 150, 145$ and 140 MeV , respectively. Therefore, all these values are in agreement with the stability window; satisfy some observational constraints for the mass and radius of observed compact stars, as discussed below, and are in agreement with the Bayesian analysis presented in Ref. [17]. Also, it is important to explain that the values of the bag constant are very near each other, so we easily see that the effect on the EoS, stellar masses, and gravitational frequencies are, mainly, due to the G_V parameter.

Another important quantity is the speed of sound of SQM, v_s , which provides information about the stiffness of the EoS related to the microscopic degrees of freedom of the model at hand. This in turn affects static and dynamic stellar observables [19] such as tidal deformabilities and gravitational-wave signatures, respectively. Its square (for catalyzed matter) is defined as:

$$v_s^2 = \frac{dp}{d\epsilon}. \quad (11)$$

We display in Fig. 1 the EoSs and the squared speed of sound for different values of G_V .

We can see that increasing the G_V stiffens the EoS. If we choose $G_V = 0$, therefore lower values of the bag would produce stiffer EoS, but the curves would have the same inclination, only displaced in the figure. The effect of the G_V is more explicit in the speed of sound. If $G_V = 0$, then all the EoSs would have the same v_s^2 , independently of the bag value. However, as we increase G_V we also increase the speed of sound.

Moreover, in the absence of the Dirac sea [13], both, the EoSs and the speed of sound are monotonically crescent with the density. If we simulate the Dirac sea contribution via a self-interaction in the vector field, we can have a decreasing speed of sound as pointed out in Ref. [4, 17]. However, as it softens the EoS we choose not to take into account the self-interaction.

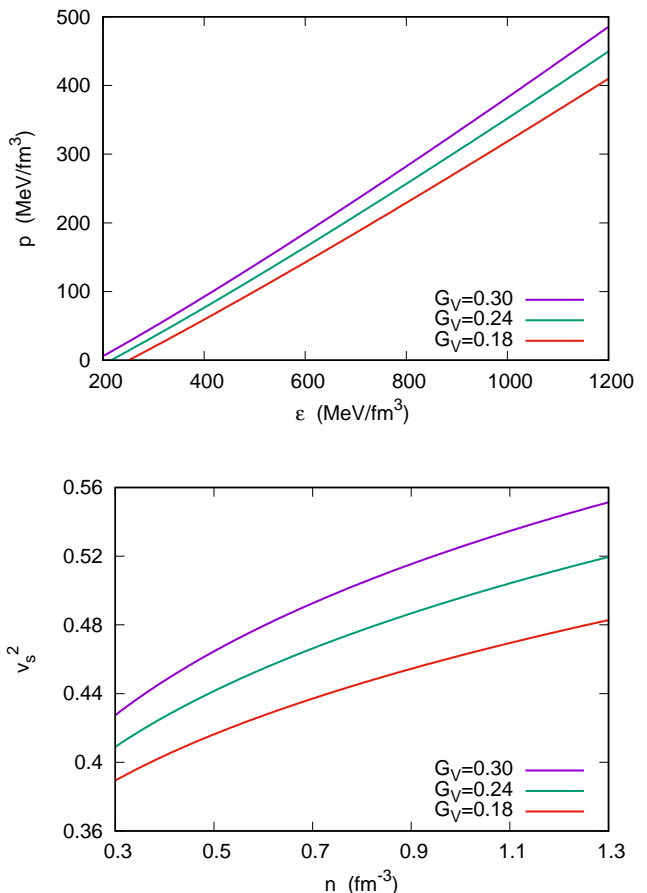


FIG. 1. (Color online) EoS (top) and the square of the speed of sound (bottom) for the three parametrizations discussed in the text.

III. CONFIGURATIONS IN RELATIVISTIC HYDROSTATIC EQUILIBRIUM

In order to study the equilibrium configuration of a relativistic star, we begin by describing the background space-time using the following static, spherically symmetric line element given by

$$ds^2 = -e^{\nu(r)} dt^2 + e^{\lambda(r)} dr^2 + r^2(d\theta^2 + \sin^2\theta d\phi^2), \quad (12)$$

where t , r , θ and ϕ are the set of Schwarzschild-like coordinates, and the metric potentials $\nu(r)$ and $\lambda(r)$ are functions of the radial coordinate r . This metric is used to compute the Einstein tensor $G_{\mu\nu}$. Then, we consider the energy-momentum tensor of a perfect fluid

$$T_{\mu\nu} = (\epsilon + p)u_\mu u_\nu + pg_{\mu\nu}, \quad (13)$$

where u_μ is the fluid 4-velocity and ‘ ϵ ’ and ‘ p ’ are the energy density and pressure, respectively. Finally, we put the Einstein tensor $G_{\mu\nu}$ and this energy-momentum tensor into the Einstein field equations (in geometrical units)

$$G_{\mu\nu} = 8\pi T_{\mu\nu}, \quad (14)$$

to obtain the Tolman-Oppenheimer-Volkoff (TOV) equations [20, 21]

$$\frac{dm}{dr} = 4\pi r^2 \epsilon, \quad (15)$$

$$\frac{d\nu}{dr} = -\frac{2}{\epsilon} \frac{dp}{dr} \left(1 + \frac{p}{\epsilon}\right)^{-1}, \quad (16)$$

$$\frac{dp}{dr} = -\frac{\epsilon m}{r^2} \left(1 + \frac{p}{\epsilon}\right) \left(1 + \frac{4\pi p r^3}{m}\right) \left(1 - \frac{2m}{r}\right)^{-1} \quad (17)$$

where m is the gravitational mass inside the radius r . These equations allow us obtain the stellar configuration in hydrostatic equilibrium and they will be used in this work for two main purposes. The first consists in determining the stellar masses and radii, while the second is aimed to study the behavior of physical quantities within the star, such as the pressure, energy density, speed-of-sound and metric radial profiles.

It is important to note that the metric function ν satisfies the following boundary condition

$$\nu(r = R) = \ln \left(1 - \frac{2M}{R}\right), \quad (18)$$

where M and R are the mass and radius for a given SQM star, respectively. With this condition, the metric function will match smoothly to the Schwarzschild metric outside the star according to the Birkhoff's theorem. The boundary conditions are $m(r = 0) = 0$ and $p(r = R) = 0$.

We show in Fig. 2 the resulting M - R relation obtained by solving the TOV equations. We also discuss some constraints present in the literature. The first one is related to the radius of the $1.4 M_\odot$ canonical neutron star. Two NICER teams have pointed the stellar radius to a limit of 13.85 km [22] and 14.26 km [23]. These results were refined in Ref. [24] to $11.80 \text{ km} < R_{1.4} < 13.10 \text{ km}$. This constraint is represented by a narrow blue strip. Very close to this canonical mass, the mass and radius of the PSR J0437–4715 were recently constrained by one of the NICER teams in Ref. [25]. The authors pointed out a mass of $M = 1.418 \pm 0.037 M_\odot$ and a radius in the range $R = 11.36^{+0.95}_{-0.63} \text{ km}$, which presents a strong constraint for traditional hadronic stars. A black strip represents this astrophysics bound. Another important constraint is the well-established existence of very massive pulsars, with $M > 2.0 M_\odot$. The more prominent example is the PSR J0740+6620 studied by two NICER teams, whose gravitational mass is $2.08 \pm 0.07 M_\odot$ with a radius lying in the range $R = 12.39^{+1.30}_{-0.98} \text{ km}$ [24, 26]. This constraint is presented as an orange-hatched area. Finally, in the realm of very light objects, the proper existence of the so-called HESS J1731-347 supernova remnant present a puzzle once it has a unique mass of $M = 0.77^{+0.20}_{-0.17} M_\odot$ and a radius $R = 10.4^{+0.86}_{-0.78} \text{ km}$ [27]. This constraint is presented as a yellow-hatched area.

We can see that while the HESS object presents a challenge for standard hadronic models, it can easily fit as a strange quark star. The three values of G_V utilized in

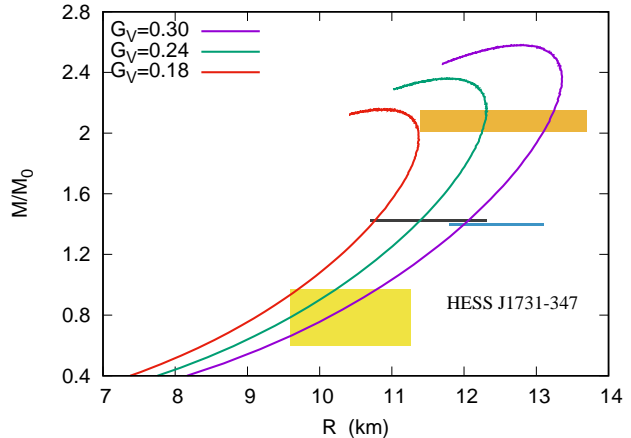


FIG. 2. Mass-radius diagram (M_\odot is the Sun's mass) for SQM stars obtained by solving the TOV equations for the three parameterizations and constraints discussed in the main text.

this work are able to fulfill such constraints. The same is true for the radius of the PSR J0437–4715. On the other hand, the radius of the canonical star presented in Ref. [24], can only be satisfied for $G_V = 0.30 \text{ fm}^2$. For lower values of the G_V , the radius of the $1.4 M_\odot$ is lower than 11.80 km. Finally, in the case of the PSR J0740+6620 with a mass of $2.08 \pm 0.07 M_\odot$, the $G_V = 0.18$ cannot satisfy it. Although it predicts a maximum mass of $2.16 M_\odot$, all stars with $M > 2.0 M_\odot$ have a radius below 11.4 km. Ultimately, only $G_V = 0.30 \text{ fm}^2$ can simultaneously fulfill all these four constraints.

Another observable predicted by Einstein's general relativity is the gravitational redshift 'z' which represents the fractional change between the observed (at infinity) and emitted (at the surface) wavelengths compared to the emitted wavelength. For a TOV star, it is given by [28]:

$$z = \left(1 - \frac{2M}{R}\right)^{-1/2} - 1. \quad (19)$$

The results for the gravitational redshift of SQM stars from the vMIT model as a function of their masses are shown in Fig. 3 for different values of G_V . First, it is clear that the redshift enlarges as the total mass of the strange quark star grows. Second, it is easily seen that the redshift value strongly depends on G_V . Lower values of G_V produce more compact stars, and consequently, larger values of z . Thus, by increasing the value of G_V , the redshift slightly decreases for SQM stars whose masses are less than $1 M_\odot$. As the mass of the stars grows, the differences in the redshift between each curve become more noticeable. When a strange quark star family approaches its maximum mass on each curve, they share almost the same value of z , although with different values of M .

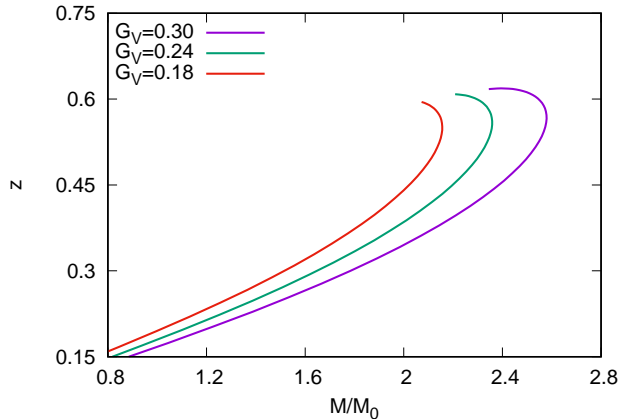


FIG. 3. The gravitational redshift ‘ z ’ versus the SQM star’s mass M (M_0 is the Sun’s mass) for different values of G_V .

IV. RADIAL OSCILLATIONS

Radial oscillations are of significant interest in neutron star seismology because, for a star to exist, it must remain stable against radial perturbations. If the star becomes unstable, it could either explode or collapse, potentially forming a black hole. This underscores the importance of studying radial oscillations, and indeed, many studies exist on this subject, e.g. Refs. [29–31].

In order to analyze the radial oscillations of a self-bound star, we first need to establish its stellar configuration in hydrostatic equilibrium, as discussed in the previous section. Next, we apply an infinitesimal and radial disturbance (perturbation) to this configuration which keeps the star’s spherical symmetry. These perturbations are introduced into the Einstein field equations, along with the conservation equations for energy, momentum, and baryon number. This process yields an Sturm-Liouville problem for the radial displacements [32].

Chronologically, this eigenvalue problem was originally derived by S. Chandrasekhar [32] and later reformulated by Chanmugan [33] in a format particularly well-suited for numerical applications, although with unintuitive boundary conditions. Two key quantities that describe these pulsations are the relative radial displacement, $\xi = \Delta r/r$, where Δr represents the radial displacement of a matter element and $\Delta p/p$, where Δp is the Lagrangian perturbation of pressure. Instead, in this work, we use the set of equations of Gondek et al. [34, 35] which is also a pair of differential equations which work nicely numerically due to the explicit use of Δp as an unknown Lagrangian variable to be determined after applying intuitive boundary conditions. The equations read

$$\frac{d\xi}{dr} = -\frac{1}{r} \left(3\xi + \frac{\Delta p}{\gamma p} \right) - \frac{dp}{dr} \frac{\xi}{(p + \epsilon)}, \quad (20)$$

$$\begin{aligned} \frac{d\Delta p}{dr} = & \xi \left\{ \omega^2 e^{\lambda - \nu} (p + \epsilon) r - 4 \frac{dp}{dr} \right\} \\ & + \xi \left\{ \left(\frac{dp}{dr} \right)^2 \frac{r}{(p + \epsilon)} - 8\pi e^\lambda (p + \epsilon) p r \right\} \\ & + \Delta p \left\{ \frac{dp}{dr} \frac{1}{(p + \epsilon)} - 4\pi (p + \epsilon) r e^\lambda \right\}, \quad (21) \end{aligned}$$

where γ is the relativistic adiabatic index, given by

$$\gamma = \frac{(\epsilon + p)}{p} \left(\frac{dp}{d\epsilon} \right), \quad (22)$$

ω represents the eigenfrequency, and the quantities $\xi \equiv \Delta r/r$ and Δp are assumed to vary harmonically with time as $e^{i\omega t}$.

To solve equations (20) and (21) one needs two boundary conditions. The first is the condition of regularity at the center ($r = 0$), which can be written as [34, 36, 37]

$$(\Delta p)_{\text{center}} = -3(\xi \gamma p)_{\text{center}}, \quad (23)$$

where the eigenfunctions are normalized in order to have $\xi(0) = 1$. The second boundary condition expresses the fact that the Lagrangian perturbation in the pressure at the stellar surface is zero

$$(\Delta p)_{\text{surface}} = 0, \quad (24)$$

this condition arises from the requirement that the pressure reaches zero at the surface $p(r = R) = 0$.

To numerically solve the oscillation equations, we proceed as follows. First, we choose a central pressure and integrate the Tolman-Oppenheimer-Volkoff (TOV) equations to obtain the stellar mass, radius, and also, the coefficients of the oscillation equations. Next, we apply the shooting method to solve the oscillation equations: starting with a trial value of ω^2 , we numerically integrate Eqs. (20) and (21) using the initial values of $\xi(r = 0)$ and $\Delta p(r = 0)$ that satisfy the central boundary condition outlined above. The integration proceeds outward, with the aim of matching the boundary condition at the star’s surface. After each integration, the trial value of ω^2 is adjusted to improve the level of precision. The discrete values of ω^2 that satisfy Eq. (24) under these conditions are identified as the eigenfrequencies of the radial perturbations. For more details on the method see Ref. [35]. In this section, for reasons of coherence, we call ν_0 the numerical value of the frequency of the fundamental radial mode.

In Fig. 4 we show our results for the radial f -mode frequency, ν_0 , as a function of the gravitational mass M for different values of G_V . We can see that for stars with masses in the interval of approximately $(1.2 - 2.0) M_\odot$, the increase in the G_V parameter produces an increase

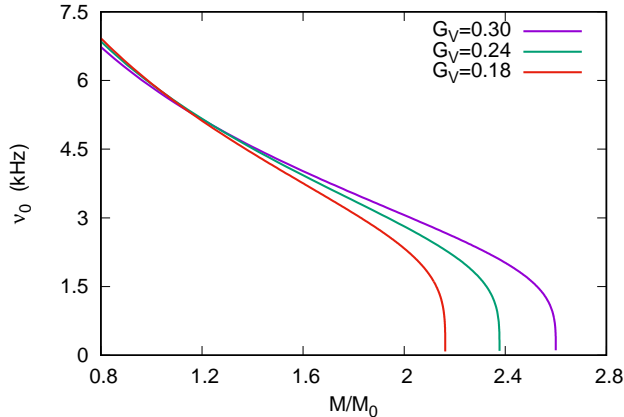


FIG. 4. The f -mode frequency (ν_0) versus the gravitational mass M (M_0 is the Sun's mass) for different values of G_V .

in the value of the fundamental radial mode. However, the increase in the G_V parameter has the opposite effect below $1.2 M_\odot$. We also observe that an increase in this parameter produces a shift to the right of all the massive stellar models, thus explaining why it is possible to obtain more massive and stable stars. In fact, the increase in the parameter G_V is related to the increase in mass, which can also be explained in terms of its stabilizing properties from a microscopic point of view. Therefore, we can conclude that increasing values of the G_V parameter allow for more massive and dynamically stable massive self-bound stars obtained from the vMIT model.

We can also observe that the frequency reaches the zero value at the point where the models attain their maximum mass, as expected for one-phase stars. In contrast, if one allowed for a thin hadronic crust (not violating the Bodmer-Witten hypothesis), a discontinuous phase-transition-like phenomenon might occur near the stellar surface. However, since this crust is extremely thin, the whole stellar stability results for this radial f -mode will not be modified. Besides, our radial-oscillation calculation agrees with the static condition which only depends on the TOV solutions [29]. In a future study, we plan to explore the presence of strong phase transitions inside neutron stars, but now using our vMIT model. This is because a recent work offers an alternative explanation for the low-mass ultracompact star HESS J1731-347, i.e. the authors of Ref. [38] consider that this object has a phase transition potentially connected to quark deconfinement.

V. NON-RADIAL OSCILLATIONS

We now pass to study the non-radial perturbations of our self-bound stars obtained from the vMIT but only by focusing on the f -mode. It is worth to mention that we solve the full dynamical (time-dependent) problem

within first-order perturbation theory without assuming any simplification such as the Cowling approximation.

Somewhat similar as in the radial case, we start now by applying polar non-radial perturbations to a non-rotating perfect fluid star giving a set of coupled equations [39]. In this formalism, the perturbed metric tensor reads

$$ds^2 = -e^\nu(1 + r^\ell H_0 Y_m^\ell e^{i\omega t})dt^2 - 2i\omega r^{\ell+1} H_1 Y_m^\ell e^{i\omega t} dt dr + e^\lambda(1 - r^\ell H_0 Y_m^\ell e^{i\omega t})dr^2 + r^2(1 - r^\ell K Y_m^\ell e^{i\omega t})(d\theta^2 + \sin^2 \theta d\phi^2), \quad (25)$$

where H_0, H_1, K are metric perturbation functions and ω is the angular frequency.

The polar perturbations in the position of the fluid elements are given by the following Lagrangian displacements

$$\xi^r = r^{\ell-1} e^{-\lambda/2} W Y_m^\ell e^{i\omega t}, \quad (26)$$

$$\xi^\theta = -r^{\ell-2} V \partial_\theta Y_m^\ell e^{i\omega t}, \quad (27)$$

$$\xi^\phi = -r^\ell (r \sin \theta)^{-2} V \partial_\phi Y_m^\ell e^{i\omega t}, \quad (28)$$

where W and V are fluid perturbation functions. In the equations above Y_m^ℓ are the spherical harmonics.

Using the previous quantities and putting them inside the perturbed Einstein equations, we can obtain the following set of first-order linear differential equations that govern the non-radial oscillations of the star [39]:

$$H_1' = -r^{-1}[\ell + 1 + 2me^\lambda/r + 4\pi r^2 e^\lambda(p - \epsilon)]H_1 + e^\lambda r^{-1}[H_0 + K - 16\pi(\epsilon + p)V], \quad (29)$$

$$K' = r^{-1}H_0 + \frac{\ell(\ell+1)}{2r}H_1 - \left[\frac{(\ell+1)}{r} - \frac{\nu'}{2}\right]K - 8\pi(\epsilon + p)e^{\lambda/2}r^{-1}W, \quad (30)$$

$$W' = -(\ell+1)r^{-1}W + re^{\lambda/2}[e^{-\nu/2}\gamma^{-1}p^{-1}X - \ell(\ell+1)r^{-2}V + \frac{1}{2}H_0 + K], \quad (31)$$

and

$$X' = -\ell r^{-1}X + \frac{(\epsilon + p)e^{\nu/2}}{2} \left[(r^{-1} + \nu'/2) H_0 + \left(r\omega^2 e^{-\nu} + \frac{\ell(\ell+1)}{2r} \right) H_1 + \left(\frac{3}{2}\nu' - r^{-1} \right) K - \ell(\ell+1)r^{-2}\nu'V - 2r^{-1} \left(4\pi(\epsilon + p)e^{\lambda/2} + \omega^2 e^{\lambda/2-\nu} - \frac{r^2}{2}(e^{-\lambda/2}r^{-2}\nu')' \right) W \right], \quad (32)$$

where the prime denotes a derivative with respect to the radial coordinate ' r ' and ' γ ' is again the adiabatic index. Also, in the equations above, the function X is given by

$$X = \omega^2(\epsilon + p)e^{-\nu/2}V - \frac{p'}{r}e^{(\nu-\lambda)/2}W + \frac{1}{2}(\epsilon + p)e^{\nu/2}H_0, \quad (33)$$

and H_0 fulfills the algebraic relation

$$a_1 H_0 = a_2 X - a_3 H_1 + a_4 K, \quad (34)$$

with

$$a_1 = 3m + \frac{1}{2}(l+2)(l-1)r + 4\pi r^3 p, \quad (35)$$

$$a_2 = 8\pi r^3 e^{-\nu/2}, \quad (36)$$

$$a_3 = \frac{1}{2}l(l+1)(m + 4\pi r^3 p) - \omega^2 r^3 e^{-(\lambda+\nu)}, \quad (37)$$

$$a_4 = \frac{1}{2}(l+2)(l-1)r - \omega^2 r^3 e^{-\nu} - r^{-1} e^\lambda (m + 4\pi r^3 p)(3m - r + 4\pi r^3 p). \quad (38)$$

Outside the star, i.e. the vacuum, $m = M$, the perturbations equations on the fluid are null and the differential equations reduce to the very well-known Zerilli equations, which can be expressed as follows

$$\frac{d^2 Z}{dr^{*2}} = [V_Z(r^*) - \omega^2]Z, \quad (39)$$

where $Z(r^*)$ and $dZ(r^*)/dr^*$ are related to the metric perturbations $H_0(r)$ and $K(r)$ by the transformations given in Refs. [39, 40]. We can also note the ‘‘tortoise’’ coordinate given by

$$r^* = r + 2M \ln(r/(2M) - 1), \quad (40)$$

and the effective potential $V_Z(r^*)$ is given by

$$V_Z(r^*) = \frac{(1 - 2M/r)}{r^3(nr + 3M)^2} f(r), \quad (41)$$

where

$$f(r) = [2n^2(n+1)r^3 + 6n^2Mr^2 + 18nM^2r + 18M^3] \quad (42)$$

with $n = (l-1)(l+2)/2$.

The system of Eqs. (29)–(32) has four linearly independent solutions for given values of l and ω . In particular, we restrict ourselves to the $l = 2$ component, which dominates the emission of gravitational waves.

The physical solution needs to verify the following appropriate boundary conditions:

- The perturbation functions: H_1, K, W and X , must be finite everywhere, particularly at $r = 0$. To implement such a condition, it is necessary to use a power series expansion of the solution near the singular point $r = 0$. The procedure is explained in detail in Refs. [39, 40].
- The next boundary condition says that the Lagrangian perturbation in the pressure has to be zero at the surface of the star $r = R$. This implies that the function X must vanish at $r = R$.
- And finally, outside the star, the perturbed metric describes a combination of outgoing and ongoing gravitational waves. The physical solution of the Zerilli equation is the one that describes purely outgoing gravitational radiation at $r = \infty$.

Such boundary conditions cannot be verified by any value of ω and the frequencies that fulfill this requirement represent the quasinormal modes of the stellar model. Now we proceed to give our findings for these non-radial f -mode frequencies as well as their damping times τ [41]. The damping time, in the context of non-radial oscillations in compact stars, represents the characteristic timescale over which the energy of these oscillations dissipates. This dissipation is primarily driven by mechanisms such as gravitational wave emission, viscosity, and neutrino radiation. The damping time has a direct impact on the detectability of gravitational waves generated by oscillating compact stars. Short damping times result in a rapid decay of the gravitational wave signal, whereas longer damping times allow the signal to persist over extended periods, improving its likelihood of detection. In the era of advanced gravitational wave observatories like LIGO and Virgo, the damping time is a key parameter in modeling and interpreting signals from neutron stars and other compact objects. Within the theoretical framework, it is essential to emphasize that the damping time cannot be determined using the Cowling approximation [42].

In the top panel of Fig. 5 we show these f -mode frequencies. As it was explained in previous sections, our analysis considered three particular constant values of the parameter G_V corresponding to the vMIT bag model. We can see that the increase in the G_V parameter shifts the curves to the lower region of the figure. From this figure, it is also obvious that for masses below $2 M_\odot$, the f -mode frequencies behave linearly with the gravitational mass. For SQM stars with masses in the range $2.0 M_\odot - 2.4 M_\odot$, the f -mode curves upwards, i.e. the f -mode frequencies start to rise noticeably until the maximum mass of the stellar models is reached. It is important to mention that the NICER teams and the observations of the HESS object imposed strong restrictions and then the value $G_V = 0.30 \text{ fm}^2$ fulfills astronomical observations. Therefore, the constrained value of this parameter also imposes restrictions on the non-radial oscillations and gravitational frequencies. Then we can see that the frequency of the fundamental mode is restricted to (1.6 - 1.8) kHz for high mass stars and to (1.5 - 1.6) kHz for low mass stars.

Furthermore, we show the damping time τ for the f -mode in the lower panel of Fig. 5. One can see that the effect of the G_V parameter has similar effects in the curves. For instance, near to the maximum mass of the stellar models, the f -mode curves downwards. The only difference is that this bending is more abrupt when compared to other work reported in the literature [42, 43]. We also observe that an increase in the values of G_V produces a systematic increase in the damping time, thus shifting the curves to the upper region of this figure.

To finish our analyses, we investigate the universal relation between the f -mode frequency, and the square root of the average density, $(M/R^3)^{1/2}$. It was pointed out in Ref. [44] that in the Newtonian limit of the theory of

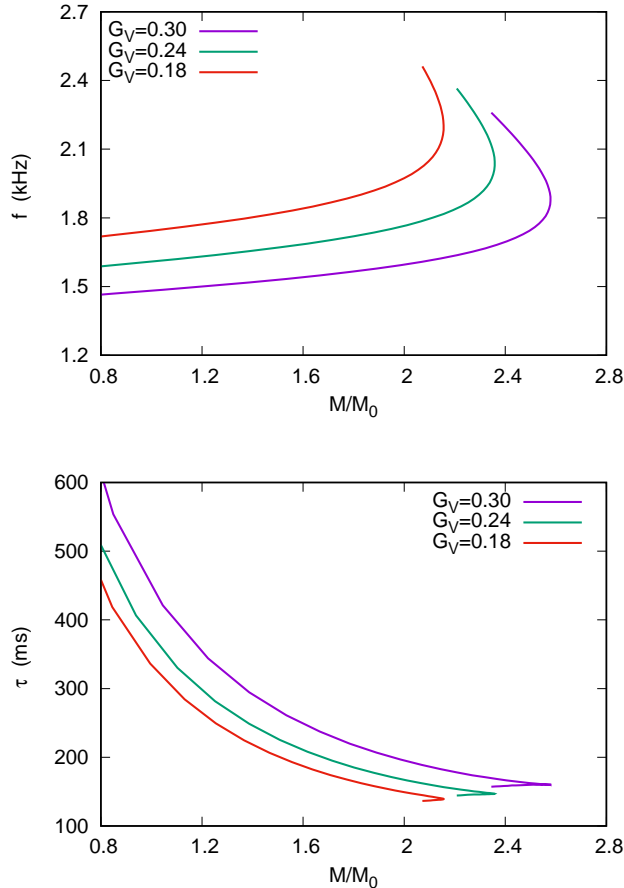


FIG. 5. Non-radial f -mode frequencies (top) and damping time (bottom) versus the mass M for different values of G_V .

stellar perturbations, the f -mode frequency scales as the square root of the average density; and the f -mode can be fitted by the following linear expression:

$$f = a + b \cdot (M/R^3)^{1/2}, \quad (43)$$

where a is given in kHz and b in $\text{km} \times \text{kHz}$. The results are displayed in Fig. 6.

We observe that the linear relation between f and the square root of the average density is not only kept, but they present very similar coefficients, yet they cover different ranges of f . We obtain $a = +0.142, +0.107,$ and $+0.009$ kHz, $b = 41.1, 42.3,$ and 44.2 $\text{km} \times \text{kHz}$ for $G_V = 0.30, 0.24$ and 0.18 fm^2 respectively.

VI. CONCLUSIONS

As we discussed in our work, we have used the vector MIT model in order to verify the QM hypothesis, and as a consequence, it is possible to see that there exists little freedom for the bag constant B once the G_V parameter is

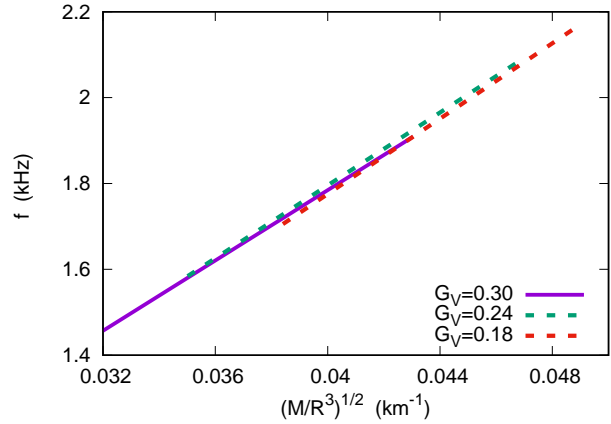


FIG. 6. The frequency of the fundamental mode is plotted in the upper panel as a function of the square root of the average density for the different EoSs. The linear relation is satisfied for all three EoSs.

selected, i.e all the results can be explained as a function of the G_V parameter alone. It is important to mention that these parameter values are in agreement with recent astronomical observations.

Then, once we have selected the G_V parameters, we explored the effect, of the vector field exchange term, on the mass and radius of strange quark stars. We have seen that the supernova remnant HESS J1731-347, and the PSR J0437-4715 are satisfied by the three G_V parameters. But although we can always produce massive stars, with $M > 2.0M_\odot$, the radius of the PSR J0740-6620 is satisfied only by $G_V = 0.30$ and 0.24 fm^2 . We have found even more restrictions due to the radius of the canonical star, and finally, we concluded that $G_V = 0.30$ fm^2 agrees with all constraints. Concerning the redshift z , we see that massive stars have a higher value of z . Moreover, for a fixed mass value, low values of G_V produce a higher value of z . The redshift of the maximum massive star is almost the same for all values the G_V , although the masses are different.

In the sequence, we have studied the radial oscillations, because they are very important as a dynamical and strong test for the stability of a compact object. As a main conclusion we have seen that the increase in the G_V parameter has a stabilizing property for stars in the range $(1.2 - 2.0)M_\odot$ but for stars below $1.2 M_\odot$ we have the opposite effect.

Finally, we studied the non-radial oscillations of strange quark stars. Recall that our results for the mass and radius of the astronomical observations have implicitly selected the G_V parameter to the 0.30 fm^2 values. Then, as a main consequence, the gravitational wave frequency of the fundamental mode is restricted to $(1.6 - 1.8)$ kHz for high mass stars and to $(1.5 - 1.6)$ kHz for low mass stars. We also show that the linear relation between the f -mode and the square root of the average density expressed in Eq. 43 is satisfied for all EoS studied.

Acknowledgements: L.L.L. was partially supported by CNPq Universal Grant No. 409029/2021-1. L.B.C. was partially supported by CNPq, Brazil under grants 308172/2023-0, FAPEMA and CAPES - Finance code 001. C. Flores acknowledges the financial support of

the productivity program of the Conselho Nacional de Desenvolvimento Científico e Tecnológico (CNPq), with Project No. 304569/2022-4. J.C.J. is supported by Conselho Nacional de Desenvolvimento Científico e Tecnológico (CNPq) with Grant No. 151390/2024-0.

-
- [1] A. R. Bodmer, Collapsed nuclei, *Phys. Rev. D* **4**, 1601 (1971).
- [2] E. Witten, Cosmic separation of phases, *Phys. Rev. D* **30**, 272 (1984).
- [3] L. Lopes, C. Biesdorf, and D. Menezes, Modified mit bag models—part i: Thermodynamic consistency, stability windows and symmetry group, *Phys. Scr.* **96**, 065303 (2021).
- [4] L. L. Lopes *et al.*, Modified mit bag models—part ii: Qcd phase diagram and hot quark stars, *Phys. Scr.* **96**, 065302 (2021).
- [5] H. T. Cromartie *et al.* (NANOGrav), Relativistic Shapiro delay measurements of an extremely massive millisecond pulsar, *Nature Astron.* **4**, 72 (2019), 1904.06759.
- [6] B. P. Abbott *et al.* (LIGO Scientific, Virgo), GW170817: Observation of Gravitational Waves from a Binary Neutron Star Inspiral, *Phys. Rev. Lett.* **119**, 161101 (2017), arXiv:1710.05832 [gr-qc].
- [7] M. Branchesi *et al.*, Science with the Einstein Telescope: a comparison of different designs, *JCAP* **2023** (07), 068.
- [8] M. Evans *et al.*, A Horizon Study for Cosmic Explorer: Science, Observatories, and Community, arXiv (2021), 2109.09882 [astro-ph.IM].
- [9] M. Colpi *et al.*, LISA Definition Study Report, arXiv (2024), 2402.07571 [astro-ph.CO].
- [10] C. Flores, L. Lopes, L. Benito, and D. Menezes, Gravitational wave signatures of highly magnetized neutron stars, *The European Physical Journal C* **80**, 1142 (2020).
- [11] A. Chodos, R. L. Jaffe, K. Johnson, C. B. Thorn, and V. F. Weisskopf, New extended model of hadrons, *Phys. Rev. D* **9**, 3471 (1974).
- [12] B. D. Serot, Quantum hadrodynamics, *Rep. Progr. Phys.* **55**, 1855 (1992).
- [13] R. Furnstahl, B. D. Serot, and H.-B. Tang, Vacuum nucleon loops and naturalness, *Nucl. Phys. A* **618**, 446 (1997).
- [14] R. O. Gomes, V. Dexheimer, S. Han, and S. Schramm, Can magnetic fields (de)stabilize twin stars?, *Mont. Not. Roy. Astron. Soc.* **485**, 4873 (2019).
- [15] R. O. Gomes, P. Char, and S. Schramm, Constraining strangeness in dense matter with gw170817, *Astrophys. J.* **877**, 139 (2019).
- [16] B. Franzon, R. O. Gomes, and S. Schramm, Effects of the quark-hadron phase transition on highly magnetized neutron stars, *Mon. Not. Roy. Astron. Soc.* **463**, 571 (2016).
- [17] F. M. da Silva *et al.*, Bayesian study of quark models in view of recent astrophysical constraints, *Phys. Rev. D* **109**, 043054 (2024).
- [18] C. Biesdorf, L. L. Lopes, and D. P. Menezes, Qcd phase diagrams via qhd and mit-based models, *Braz. J. Phys.* **53**, 137 (2023).
- [19] S. Altiparmak, C. Ecker, and L. Rezzolla, On the Sound Speed in Neutron Stars, *Astrophys. J. Lett.* **939**, L34 (2022).
- [20] R. C. Tolman, Static solutions of einstein’s field equations for spheres of fluid, *Phys. Rev.* **55**, 364 (1939).
- [21] J. R. Oppenheimer and G. M. Volkoff, On massive neutron cores, *Phys. Rev.* **55**, 374 (1939).
- [22] T. E. Riley *et al.*, A NICER View of PSR J0030+0451: Millisecond Pulsar Parameter Estimation, *Astrophys. J. Lett.* **887**, L21 (2019).
- [23] M. Miller *et al.*, PSR J0030+0451 Mass and Radius from NICER Data and Implications for the Properties of Neutron Star Matter, *Astrophys. J. Lett.* **887**, L24 (2019).
- [24] M. Miller *et al.*, The radius of PSR j0740+6620 from NICER and XMM-newton data, *Astrophys. J. Lett.* **918**, L28 (2021).
- [25] D. Choudhury *et al.*, A nicer view of the nearest and brightest millisecond pulsar, arXiv:2407.06789 [astro-ph.HE].
- [26] T. Riley *et al.*, A nicer view of the massive pulsar psr j0740+6620 informed by radio timing and xmm-newton spectroscopy, *Astrophys. J. Lett.* **918**, L27 (2021).
- [27] V. Doroshenko, V. Suleimanov, G. Pühlhofer, and A. Santangelo, A strangely light neutron star within a supernova remnant, *Nat. Astron.* **6**, 1444 (2022).
- [28] L. L. Lopes, The neutron star inner crust: An empirical essay, *Europhys. Lett.* **134**, 52001 (2021).
- [29] J. P. Pereira, C. V. Flores, and G. Lugones, Phase Transition Effects on the Dynamical Stability of Hybrid Neutron Stars, *Astrophys. J.* **860**, 12 (2018), arXiv:1706.09371 [gr-qc].
- [30] J. D. V. Arbañil, G. A. Carvalho, R. V. Lobato, R. M. Marinho, and M. Malheiro, Extra dimensions’ influence on the equilibrium and radial stability of strange quark stars, *Phys. Rev. D* **100**, 024035 (2019), arXiv:1907.07661 [gr-qc].
- [31] J. M. Z. Pretel, Equilibrium, radial stability and non-adiabatic gravitational collapse of anisotropic neutron stars, *European Physical Journal C* **80**, 726 (2020), arXiv:2008.05331 [gr-qc].
- [32] S. Chandrasekhar, The Dynamical Instability of Gaseous Masses Approaching the Schwarzschild Limit in General Relativity., *Astrophys. J.* **140**, 417 (1964).
- [33] G. Chanmugam, Radial oscillations of zero-temperature white dwarfs and neutron stars below nuclear densities., *Astrophys. J.* **217**, 799 (1977).
- [34] D. Gondek, P. Haensel, and J. L. Zdunik, Radial pulsations and stability of protoneutron stars, *Astron. Astrophys.* **325**, 217 (1997).
- [35] C. Vásquez Flores and G. Lugones, Radial oscillations of color superconducting self-bound quark stars, *Phys. Rev. D* **82**, 063006 (2010).
- [36] H. M. Vaeth and G. Chanmugam, Radial oscillations of neutron stars and strange stars, *Astron. Astrophys.* **260**, 250 (1992).
- [37] D. Gondek-Rosinska and J. L. Zdunik, Avoided cross-

- ings in radial pulsations of neutron and strange stars, *Astron. Astrophys.* **344**, 117 (1999).
- [38] M. Mariani, I. F. Ranea-Sandoval, G. Lugones, and M. G. Orsaria, Could a slow stable hybrid star explain the central compact object in HESS J1731-347?, *Phys. Rev. D* **110**, 043026 (2024), [arXiv:2407.06347 \[astro-ph.HE\]](https://arxiv.org/abs/2407.06347).
- [39] S. Detweiler and L. Lindblom, On the nonradial pulsations of general relativistic stellar models, *Astrophys. J.* **292**, 12 (1985).
- [40] J.-L. Lü and W.-M. Suen, Determining the long living quasi-normal modes of relativistic stars, *Chinese Physics B* **20**, 040401 (2011).
- [41] N. Andersson and K. D. Kokkotas, Towards gravitational wave asteroseismology, *Mon. Not. Roy. Astron. Soc.* **299**, 1059 (1998).
- [42] B. K. Pradhan, D. Chatterjee, M. Lanoye, and P. Jaikumar, General relativistic treatment of f -mode oscillations of hyperonic stars, *Phys. Rev. C* **106**, 015805 (2022).
- [43] L. L. Lopes et al., Imprints of the nuclear symmetry energy slope in gravitational wave signals emanating from neutron stars, *Phys. Rev. D* **108**, 083042 (2023).
- [44] O. Benhar, V. Ferrari, and L. Gualtieri, Gravitational wave asteroseismology reexamined, *Phys. Rev. D* **70**, 124015 (2004).